Two Roads Diverged: The Structure of Hydroxymandelate Synthase from *Amycolatopsis orientalis* in Complex with 4-Hydroxymandelate[†,‡]

June Brownlee,[§] Panqing He,[||] Graham R. Moran,[||] and David H. T. Harrison*[,§]

Department of Biochemistry and Molecular Biology, Rosalind Franklin University of Medicine and Science, 3333 Green Bay Road, North Chicago, Illinois 60064, and Department of Chemistry and Biochemistry, University of Wisconsin—Milwaukee, 3210 North Cramer Street, Milwaukee, Wisconsin 53211-3029

Received July 21, 2007; Revised Manuscript Received December 5, 2007

ABSTRACT: The crystal structure of the hydroxymandelate synthase (HMS)·Co^{2+}·hydroxymandelate (HMA) complex determined to a resolution of 2.3 Å reveals an overall fold that consists of two similar β-barrel domains, one of which contains the characteristic His/His/acid metal-coordination motif (facial triad) found in the majority of Fe^{2+}-dependent oxygenases. The fold of the α-carbon backbone closely resembles that of the evolutionarily related enzyme 4-hydroxyphenylpyruvate dioxygenase (HPPD) in its closed conformation with a root-mean-square deviation of 1.85 Å. HPPD uses the same substrates as HMS but forms instead homogentisate (HG). The active site of HMS is significantly smaller than that observed in HPPD, reflecting the relative changes in shape that occur in the conversion of the common HPP substrate to the respective HMA or HG products. The HMA benzylic hydroxyl and carboxylate oxygens coordinate to the Co^{2+} ion, and three other potential H-bonding interactions to active site residue side chains are observed. Additionally, it is noted that there is a buried well-ordered water molecule 3.2 Å from the distal carboxylate oxygen. The *p*-hydroxyl group of HMA is within hydrogen-bonding distance of the side chain hydroxyl of a serine residue (Ser201) that is conserved in both HMS and HPPD. This potential hydrogen bond and the known geometry of iron ligation for the substrate allowed us to model 4-hydroxyphenylpyruvate (HPP) in the active sites of both HMS and HPPD. These models suggest that the position of the HPP substrate differs between the two enzymes. In HMS, HPP binds analogously to HMA, while in HPPD, the *p*-hydroxyl group of HPP acts as a hydrogen-bond donor and acceptor to Ser201 and Asn216, respectively. It is suggested that this difference in the ring orientation of the substrate and the corresponding intermediates influences the site of hydroxylation.

4-Hydroxyphenylpyruvate dioxygenase (HPPD)[1] and hydroxymandelate synthase (HMS) are homologous Fe^{2+}-dependent dioxygenases that carry out highly similar reactions and use the same substrates (Scheme 1). HPPD is ubiquitous in aerobic metabolism, catalyzing the second step of tyrosine catabolism, and has been studied for many years, in part because of its unusual reaction transformation, but also due to the medical and agricultural relevance of inhibition of the enzyme (*1*). HMS is a more recent discovery that is found in relatively few bacteria and is required to synthesize hydroxyphenylglycine, a recurring skeletal component of nonproteinogenic macrocyclic peptide antibiotics such as vancomycin (*2*, *3*). Both enzymes are exceptions within a larger enzyme family known collectively as the α-keto acid-dependent oxygenases (αKAO). Generally, αKAO enzymes use three substrates, α-ketoglutarate (AKG), molecular oxygen, and a third substrate that is specific to the enzyme. Most commonly, the specific substrate is hydroxylated during catalysis, but a variety of other types of reactions are also observed (*4*). HPPD and HMS are exceptions as they use just two substrates, 4-hydroxphenylpyruvate (HPP) and dioxygen. The cofactor used by all αKAO enzymes to reduce molecular oxygen is an α-keto acid moiety that is typically supplied by AKG and is

Scheme 1

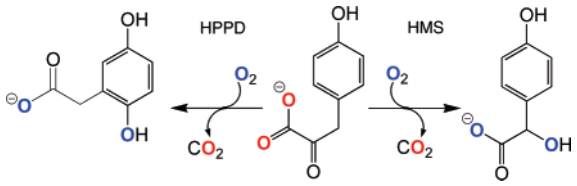

[†] This research was supported in part by National Institutes of Health Grant DK59551 to G.R.M. and a UWM Research Growth Initiative Grant to G.R.M and a Bridge Grant from Rosalind Franklin University of Medicine and Science to D.H.T.H.

[‡] Atomic coordinates of the HMS·Co^{2+}·HPP complex have been deposited in the Protein Data Bank as entry 2R5V.

* To whom correspondence should be addressed: Department of Biochemistry and Molecular Biology, Rosalind Franklin University of Medicine and Science, 3333 Green Bay Rd., North Chicago, IL 60064. E-mail: David.Harrison@rosalindfranklin.edu. Phone: (847) 578-8609. Fax: (847) 578-3240.

[§] Rosalind Franklin University of Medicine and Science.

[||] University of Wisconsin—Milwaukee.

[1] Abbreviations: HMS, hydroxymandelate synthase; αKAO, α-keto acid-dependent oxygenase; HPPD, (4-hydroxyphenyl)pyruvate dioxygenase; *Sa*HPPD, *Streptomyces avermitilis* HPPD; *Pf*HPPD, *Pseudomonas fluorescens* HPPD; *Ao*HMS, *Amycolatopsis orientalis* HMS; HPP, (4-hydroxyphenyl)pyruvate; HMA, hydroxymandelate; PPA, phenylpyruvic acid; HG, 2,5-dihydroxyphenylacetate; AKG, α-ketoglutarate; HEPES, *N*-(2-hydroxyethyl)piperazine-*N*′-2-ethanesulfonic acid; PEG, polyethylene glycol; EDTA, ethylenediaminetetraacetic acid; DFT, density functional theory; HPLC, high-performance liquid chromatography; APS, Advanced Photon Source; NCS, noncrystallographic symmetry; MOE, Molecular Operating Environment.

10.1021/bi701438r CCC: $40.75
Published on Web 01/24/2008

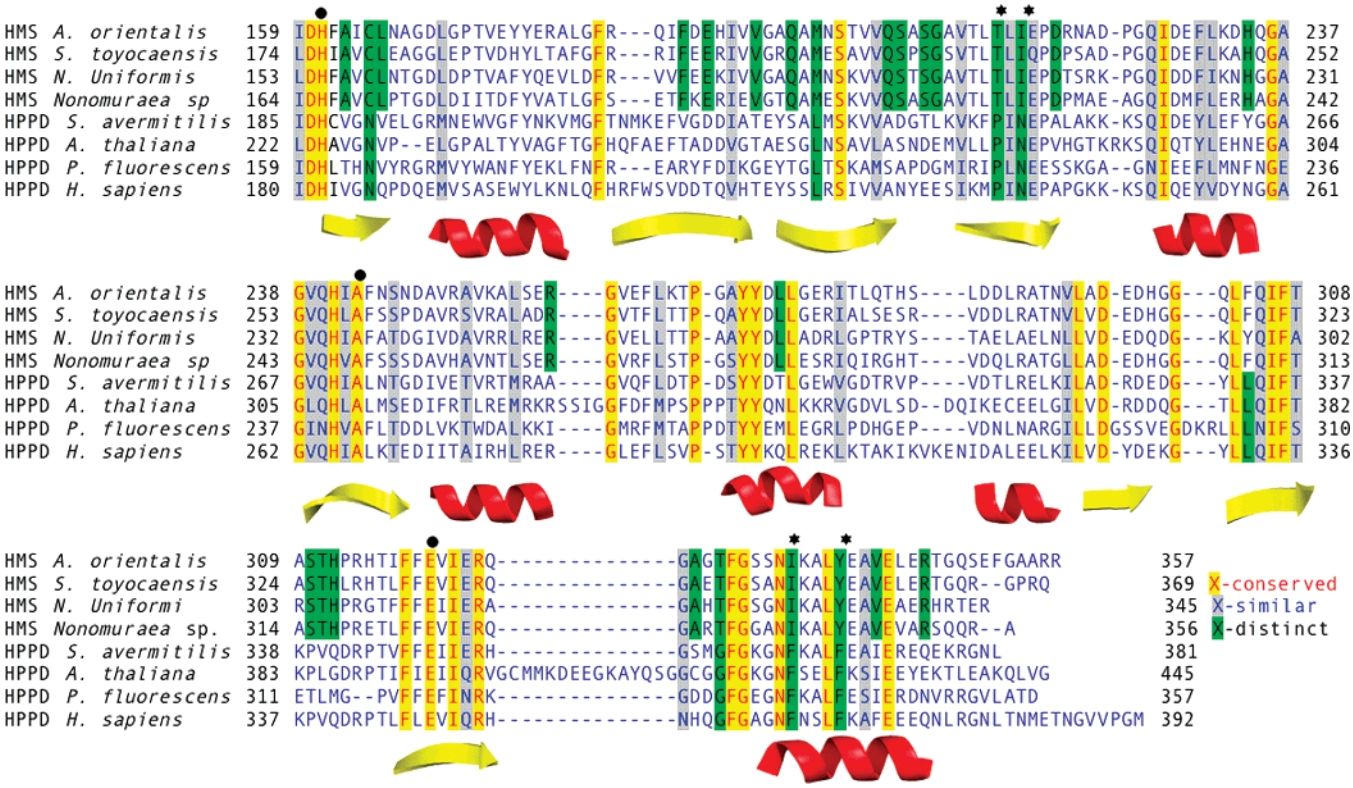

FIGURE 1: Primary structure sequence comparison of the C-terminal domains of HMS and HPPD. Fully conserved residues are highlighted in yellow, residues that have similarity in gray, and residues that are found in only HMS or HPPD in green. The positions of secondary structural elements are shown below the alignment. The residues of the facial triad that coordinate the metal ion are indicated with solid circles. The residues that have been investigated by previous mutational studies are indicated with solid stars. Blue dashes indicate gap insertions according to the primary structure alignment.

observed to coordinate to the active site ferrous ion in a bidentate fashion through the 1-carboxylate and the 2-keto groups (*5*−*10*). In the case of HPPD and HMS, the α-keto acid is a pyruvate moiety found as a substituent of the organic substrate that is ultimately hydroxylated. As such, AKG is not required for catalysis in these enzymes.

HMS and HPPD yield different products due to the site of delivery of the second oxygen atom. In the case of HPPD, the second atom of dioxygen is delivered to the aromatic ring, displacing an aceto substituent to the adjacent carbon. For HMS, the oxygen atom is directed instead to the adjacent benzylic carbon (Scheme 1). These two types of hydroxylation are fundamentally different in that aromatic hydroxylation at C1 of the ring does not involve abstraction of a hydrogen atom or hydride ion while aliphatic oxygenation of the benzylic carbon must proceed via initial abstraction from this atom. As such, there are two essential questions, is the hydroxylating intermediate the same in each case and therefore is hydroxylation regiospecificity rooted in localization and orientation of the appropriate carbon with respect to the intermediate? or, is the hydroxylating intermediate tuned to each type of reaction by active site influences other than proximity? Analysis of the C-terminal or catalytic domains of four ortholog HMS primary structures, all of which are bacterial in origin, with four representative HPPD orthologs from three kingdoms reveals a degree of sequence similarity between the two enzymes (Figure 1). Of the ∼200 C-terminal domain residues, the sequences are ∼15% identical and ∼25% similar. Residues that are conserved in only the HPPD or the HMS sequences are highlighted in green with the latter comprising 12% of the HMS residues. The similarity of the catalyzed reactions, the conservation of primary structure, and the identification of a number of enzyme-specific substitutions have led to mutagenesis studies aimed at defining which active site residues are the key determinants of positional hydroxylation specificity (*11*, *12*). These studies concentrated on four residues that surround the metal center (marked with stars in Figure 1). Gunsior et al. found that only the F337I variant of *Sa*HPPD was able to produce significant amounts of product hydroxymandelate (HMA), although at ∼0.1% of the wild-type rate. Significantly, several of the *Sa*HPPD variants made (including F337I) showed evidence of epoxide formation, and in combination (double, triple, and quadruple mutants), the overall activity of the variants diminished further without the HMS activity being enhanced. The data that are absent are the structures; neither HMS nor HPPD has hitherto been crystallized in the presence of their substrate or products, and as such, it is not known how (or if) ligand binding differs in each enzyme. In this study, we describe the structure of HMS substituted with cobalt in complex with the product HMA and compare this structure with those of HPPD.

MATERIALS AND METHODS

Materials. The apo form of HMS was expressed and purified using ammonium sulfate fractionation, anion exchange chromatography, and size exclusion chromatography according to the methods used to purify HPPD of Johnson-Winters et al. (*13*). The only part of the protocol significantly different from this published protocol was the fractional saturation used to precipitate the enzyme in that apo-HMS was precipitated in the 50−70% ammonium sulfate fraction.

PEG 3350 (50%), VDX-greased crystallization well plates, 22 mm siliconized cover slides, paratone, and paraffin were each purchased from Hampton Research. Cobalt chloride hexahydrate was purchased from Spectrum Chemicals.

Preparation and Crystallization of HMS. The initial complex of HMS·Co^{2+} with HPP was made by adding the metal (2.8 mM $CoCl_2$·$6H_2O$), and then the substrate (5.2 mM HPP), to purified apo-HMS (550 μM) in 20 mM HEPES (pH 7.0). The mixture was then allowed to incubate for 6 h at 5 °C. Initial crystallization conditions for HMS from *Amycolatopsis orientalis* were identified using the PEG/Ion Screen from Hampton Research using standard vapor diffusion "hanging-drop" methods. Crystals were ultimately grown under optimized conditions in which the well (500 μL) contained 20% PEG 3350 and 0.1 M KH_2PO_4 (pH undefined). The hanging drop (4 μL) was prepared by mixing equal volumes of the HMS·Co^{2+}·HPP complex and the well solution. The crystals that were obtained were rods with average dimensions of 70 μm × 70 μm × 500 μm and appeared within 5 days at 6 °C. Prior to data collection, crystals were transferred into a combination of paratone and paraffin oil for cryoprotection and rapidly cooled in liquid nitrogen. All crystallographic data collection was conducted at cryogenic temperatures.

Structural Determination. To obtain phase information, single-wavelength anomalous dispersion (SAD) data were collected at the APS (Argonne, IL) on the SER-CAT 22-ID beamline. The X-ray wavelength of 1.59568 Å for the cobalt absorption edge was determined by X-ray fluorescence prior to the diffraction experiment. The diffraction symmetry and systematic absences showed the crystal to belong to a primitive tetragonal space group ($P4_1$ or $P4_3$) with unit cell dimensions of 106.37 Å × 106.37 Å × 75.95 Å. These dimensions suggested that there are two protomers per asymmetric unit with a solvent content of 55%. The X-ray images were integrated, scaled, and merged to give a list of 37959 unique reflections. The data to 2.7 Å resolution were analyzed with SOLVE (*14*) to locate and refine the positions of the two cobalt atoms in the asymmetric unit to yield a mean figure of merit of 0.285. Modification of the initial phase information, including solvent flattening, histogram matching, and local pattern recognition, was performed with RESOLVE and took place iteratively with 50 rounds of RESOLVE's autobuilding/rebuilding function (*15*), resulting in an improved figure of merit of 0.68. RESOLVE confirmed the space group as $P4_1$ and located 522 amino acid residues, 294 with side chains, belonging to two protomers.

The preliminary protein model and the RESOLVE composite omit map provided the starting point for manual model building using O (*16*). Subsequent refinement was conducted with CNS (*17*), including simulated annealing and automated water picking. When data to 2.3 Å resolution were included and R_{factor} and R_{free} were 23.5 and 26%, respectively, the difference density around the metal centers was scrutinized and judged to be more consistent with HMA than HPP. On the basis of this and subsequent product analysis (vide infra), this ligand molecule was added to the model. Several more iterative rounds of refinement in O and CNS were performed, along with a final round of refinement using REFMAC 5.3 (final statistics for the structure are given in Table 1).

Verification of Ligand Identity from Product Analysis. A control reaction mixture was made by mixing 520 μM HMS, 2.8 mM $CoCl_2$·$6H_2O$, and 5.2 mM HPP in 20 mM HEPES (pH 7.0), and a second control reaction mixture was prepared without the cobaltous reagent (all concentrations final); both mixtures were allowed to incubate at 6 °C. During the following 7 days, samples from both control mixtures were withdrawn (the first after 2 h and the last after 7 days) and quenched in 3.3% (v/v) TCA (final) and centrifuged for 30 min at 14000 rpm to pellet the precipitated protein. The supernatant (40 μL) was then injected into a Waters Delta 600 HPLC unit coupled to a Phenomenex Synergi 10 μm Polar-RP 80A column (250 mm × 4.6 mm) using a 99:1 mobile phase of 20 mM citric acid (pH 3.5) and acetonitrile run isocratically at 1 mL/min. Detection was at 274 and 340 nm using a Waters 2487 dual λ absorbance detector, and chromatograms were recorded and analyzed using the PeakSimple Chromatography Data System and software (SRI). Retention times for HMA and HPP were 5.7 and 7.9 min, respectively. Prior to analysis, standard curves for HMA and HPP were constructed using the authentic compounds and the same HPLC conditions.

Modeling of Substrates in the Active Sites of HMS and HPPD. The solvent accessible cavity volumes were calculated using VOIDOO (Uppsala Software Factory). The program suite MOE (Chemical Computing Group) was used to model HPP bound to *Pf*HPPD, HMS, and *Pf*HPPD variants. Fe^{2+} ion was modeled in place of the Co^{2+} ion, and the coordinates of the facial triad were fixed, as were the protein backbone atoms. A model of HPP was positioned into the active site of HMS by superimposing the ring onto the HMA skeleton; the carbonyl oxygen and carboxylate were kept in the same plane with the modeled Fe^{2+} ion. The two oxygen−iron distances were restrained to between 1.6 and 2.4 Å, and the planarity of the keto−carboxylate system was also restrained to be consistent with the results from MCD spectroscopy (*18*). The structure was energy-minimized and subsequently subjected to 100 ps of molecular dynamics with 0.002 ps steps at a temperature of 400 K and sampled every 5 ps. The lowest-energy-sampled structure was then energy-minimized.

Table 1: Crystal Parameters and Refinement Statistics

space group	$P4_1$
cell dimensions (Å)	
a	106.37
b	106.37
c	75.95
σ cutoff	0.0
resolution range (Å)	50.0−2.30 (2.36−2.30)[a]
total no. of reflections	74249
no. of unique reflections	37953
no. of reflections used in refinement	36055
completeness (%)	99.8 (98.2)[a]
R_{sym} (%)	7.6 (32.4)[a]
R_{free} (%)	22.7 (28.3)[a]
R factor (%)	17.4 (21.1)[a]
Ramachandran most favored/additional (%)[b]	90.3/9.6
overall mean temperature factor (Å^2)	38.78
rmsd from ideal[c]	
bond lengths (Å)	0.023
bond angles (deg)	1.949

[a] Numbers in parentheses represent the last shell values. [b] Most favored and additional regions as defined by PROCHECK (*67*). [c] Root-mean-square deviations from Engh and Huber ideal values (*68*).

The structure of HPPD from *Pseudomonas fluorescens* (PDB entry 1CJX) was used to model HPP bound to HPPD. The facial triad of HPPD was aligned to the facial triad of HMS, and the modeled HPP was then inserted into the HPPD structure. The bound acetate ion was removed as was a water molecule that overlapped with the initial HPP model. Additionally, the *p*-hydroxyl group makes a bad contact with the phenyl ring of Phe337, which HPPD could resolve by using a different rotomer for this residue. This structure was then energy-minimized (which caused a substantial change in the position of Phe337). Again, the structure was subjected to 100 ps of molecular dynamics with 0.002 ps steps at a temperature of 400 K and sampled every 5 ps. The lowest-energy sampled structure was then energy-minimized.

RESULTS

Protein Expression and Purification of Apo-HMS. The T7-based expression system of Studier (*19*) was used to express HMS. On the basis of densitometry of SDS−PAGE gels, HMS expresses to 44% of total cell protein within 150 min of induction with IPTG. The enzyme was purified in four steps over a period of 48 h. These steps were streptomycin sulfate treatment to precipitate nucleic acids, ammonium sulfate fractionation, anion exchange chromatography, and size exclusion chromatography. On elution from the Q-Sepharose column, the center of the HMS peak occurred at a concentration of 420 mM NaCl. The yield of the purified enzyme from 1 L of culture was consistently ∼75 mg, and the enzyme could be stored at −80 °C indefinitely without loss of activity upon thawing. The purified enzyme contained little iron (∼0.05 Fe atom per monomer).

Overall Structure and Alignment. The asymmetric unit of HMS consists of two protomers stacked in a T-shaped arrangement with the longitudinal axis of each perpendicular to the other. The dominant protomer−protomer interface, however, occurs across a crystallographic symmetry axis into the adjacent asymmetric unit and has an area of 778 Å^2, being 5.7% of the solvent accessible surface area. This interface contains two salt bridges and nine hydrogen bonds and as such is in all probability insufficient to be regarded as being physiologically relevant, leading to the conclusion that AoHMS is a monomer in solution. The final model fit to the density map is comprised of 5297 atoms that form 676 amino acid residues and 217 solvent molecules. The overall model is ∼95% complete in that only residues A1,[2] A107−A109, A349−A357, B1, B106−B110, B129−B135, B144−B154, and B349−B357 are too disordered to model. The model has an *R* value of 17.4% (R_{free} = 22.7%), with an estimated coordinate error of 0.25 Å (*20*), and Table 1 lists the relevant crystallographic parameters of the model.

The overall fold and position of individual secondary structural elements of AoHMS are highly similar to those of the known HPPD structures (*21*−*24*) and most closely resemble the "closed" fold of HPPD from *P. fluorescens* (PfHPPD) (Figure 2). This fold uses the same tertiary structure and domain arrangement as that observed in a number of extradiol dioxygenases and is thought to have arisen from a gene duplication event (*25*, *26*). The rms deviation between the two structures is 1.85 Å for 221 closely matching α-carbons, and it is 2.1 Å for 1425 related atoms. When only residues with identity are compared (220 atoms), it is found that there is a rms deviation of 0.84 Å. When the metal and the three coordinating ligands are aligned, the rms deviation among those 28 atoms is 0.16 Å. We consider this metal center-based alignment most suitable for comparing the active sites of these two enzymes and modeling the differences in the chemical reaction. In this alignment, we note substantial differences (∼1.0−1.5 Å) in α-carbon positions for a number of residues that line the active site, including those from three *β*-strands (residues 185−194, 197−205, and 212−218) and the carboxy-terminal α-helix (residues 332−344). We also note that not only is the α-carbon of Tyr339 of HMS different by 1.6 Å relative to Phe341 of *Pf*HPPD but the tyrosine hydroxyl also points toward the bound HMA, whereas the corresponding phenylalanine ring in HPPD is pointed away from the active site.

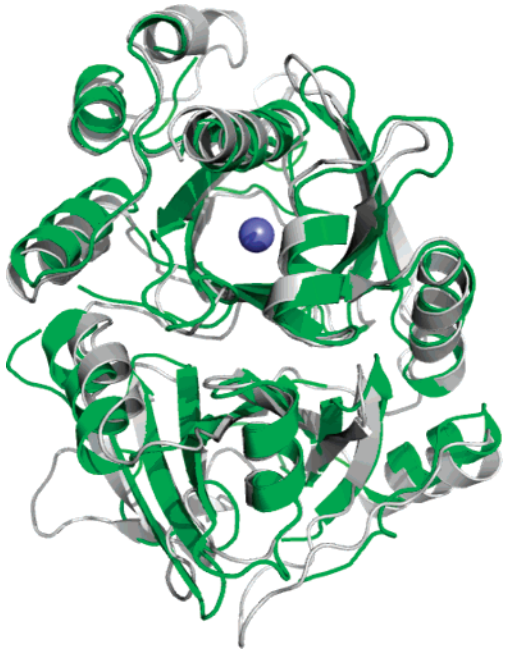

FIGURE 2: Superimposition of the ribbon representations of HMS from *A. orientalis* (green) and HPPD from *P. fluorescens* (gray).

Ligand Density and Product Analysis. The active site shows density for a ligand to the cobalt ion (Figure 3A). The form of this density was unbiased by avoiding any ligand modeling until the structural refinement of all other atoms was near completion. The ligand density has two lobes oriented at roughly 65° with respect to one another. The lobe most proximal to the cobalt clearly makes contact with the metal ion, while the remaining lobe is of the appropriate size and shape to accommodate a phenol. Crystals were grown in the presence of 5.2 mM substrate, HPP, and the structure of this molecule can be modeled, albeit unsatisfactorily, into the density map with the benzylic carbon contacting the edge of the observed density (Figure 3A, blue ligand). All of the atoms in the modeled structure of the product, HMA, fit into the electron density map without distortion and were well centered in that density (Figure 3A, light yellow ligand). To establish which of these two was actually liganding the metal

[2] The position numbers of amino acid residues used throughout this article are actual residue numbers based on the primary structure of each protein. These differ slightly from the composite numbering system used by Gunsior et al. This is most relevant for residue Phe337 from *P. fluorescens* HPPD that is numbered as 335 in the work cited.

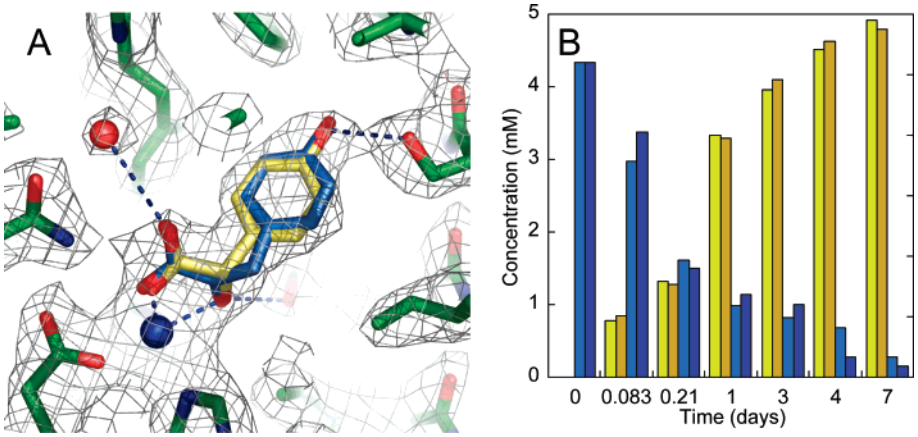

FIGURE 3: (A) Electron density map (2-1) adjacent to the active site metal ion. Both the substrate, HPP (blue), and the product, HMA (straw), are modeled into the density observed for the ligand. (B) Depletion of HPP (blue) and accumulation of HMA (straw) over the duration of the time taken to crystallize HMS when incubated under equivalent conditions. The control reaction mixture was made by mixing 520 μM HMS, 2.8 mM $CoCl_2 \cdot 6H_2O$, and 5.2 mM HPP in 20 mM HEPES (pH 7.0), and a second control reaction mixture was prepared in an equivalent manner without cobaltous ions (depicted with darker shades of color for both ligands). Both mixtures were allowed to incubate at 6 °C.

ion, product analyses were carried out on a sample of enzyme incubated under the same conditions that were used to crystallize the complex (but without precipitant).

These data show that during the time taken to form crystals, there was an ~90% conversion to HMA from the initial 5.2 mM HPP added (Figure 3B). The purification of HMS in the presence of EDTA (excluded during the final size exclusion chromatography step) led to the enzyme containing <0.05 Fe atom/ monomer. As such, 550 μM HMS would contain at most 26 μM iron. Moreover, a parallel control reaction conducted under equivalent conditions but with the exclusion of cobalt yielded a similar amount of product in the same time period, establishing that turnover did not occur in the majority fraction of the enzyme sample that is cobalt-substituted and must have resulted from trace Fe^{3+} present in reagents and the action of an unidentified reductant. The preponderance of ligand in the crystallization solution is therefore HMA.

Metal Coordination. HMA makes a distinctly asymmetric bidentate contact with the active site metal ion through one of its carboxylate oxygens (1.9 Å) and the oxygen of the hydroxyl at the benzylic carbon (2.4 Å), completing what is a distorted trigonal bipyramidal arrangement of metal ion ligands, with nitrogens from the two histidines and the oxygen of the HMA carboxylate forming the equatorial plane and the glutamate and the benzylic hydroxyl oxygens occupying apical positions (Figure 4B). No evidence of product carbon dioxide was observed. The product HMA is held in this conformation or orientation by apparent hydrogen-bonding interactions with three active site residues. The *p*-hydroxyl of HMA forms almost ideal hydrogen-bond geometry with Ser201 (with a distance of 2.7 Å), which is fully conserved in all HMS and HPPD sequences (Figure 1). The second apparent hydrogen bond extends from Thr214 to the product benzylic hydroxyl (2.9 Å). Thr214 is unique to HMS sequences and may offer a mechanistically distinguishing interaction in a substrate and/or intermediate complex for the HMS enzymes. The third potential hydrogen-bonding interaction is a donor interaction from one of the carboxylate oxygens of HMA to Gln305 (2.9 Å) that also participates as an acceptor to a nearby water molecule (*vide infra*).

Active Site Ligand Contacts. Within ~10 Å of the metal ion are 7 residues uniquely conserved in HMS and 11 residues conserved in both HMS and HPPD. Of the residues unique to HMS, all are clustered around the ligand. Ile335 makes van der Waals contacts with the phenol ring of the product (~3.4 Å) and along with Thr214, Phe188, and Ile216 forms a predominantly hydrophobic pocket in which the HMA phenol resides. Tyr339 is more distant from the phenol; however, the hydroxyl of its side chain is oriented to interact with the portion of the product that contacts the metal ion (Figure 4B). If the facial triad amino acids that coordinate the metal ion are excluded, the majority of the amino acids within the 10 Å sphere of the metal ion that are conserved in both HMS and HPPD seem to play ancillary roles in the product complex in that they are more distant and show few direct interactions with the ligand. Ser201 and Gln305 are the exceptions, and the latter is within hydrogen-bonding distance (2.5 Å) of a highly ordered water molecule, Water A. Water A is 3.2 Å from the product carboxylate and makes another potential hydrogen bond with the amide nitrogen of Gly331 which is fully conserved in all known HMS and HPPD sequences and is the hinge for the carboxy-terminal α-helix in the open and closed forms. Its proximity to the product carboxylate and the additional localizing interactions suggest a mechanistic role for this water molecule.

Modeling the HMS and HPPD Substrate Complexes. To gain insight into the structural basis for the differences in the reaction pathway with the two enzymes, substrate complexes for each were modeled using molecular dynamics simulations and energy minimization. These models suggest that differences in the orientation of the phenolic ring lead to small displacements of the α-keto acid moiety that may ultimately determine whether the benzylic or C1 aromatic carbon is exposed to attack. For the HMS·Fe^{2+}·HPP complex, the carboxylate and *p*-hydroxyl oxygen positions of HPP are essentially unchanged from those of HMA, with the *p*-hydroxyl oxygen donating a hydrogen bond to Ser201.

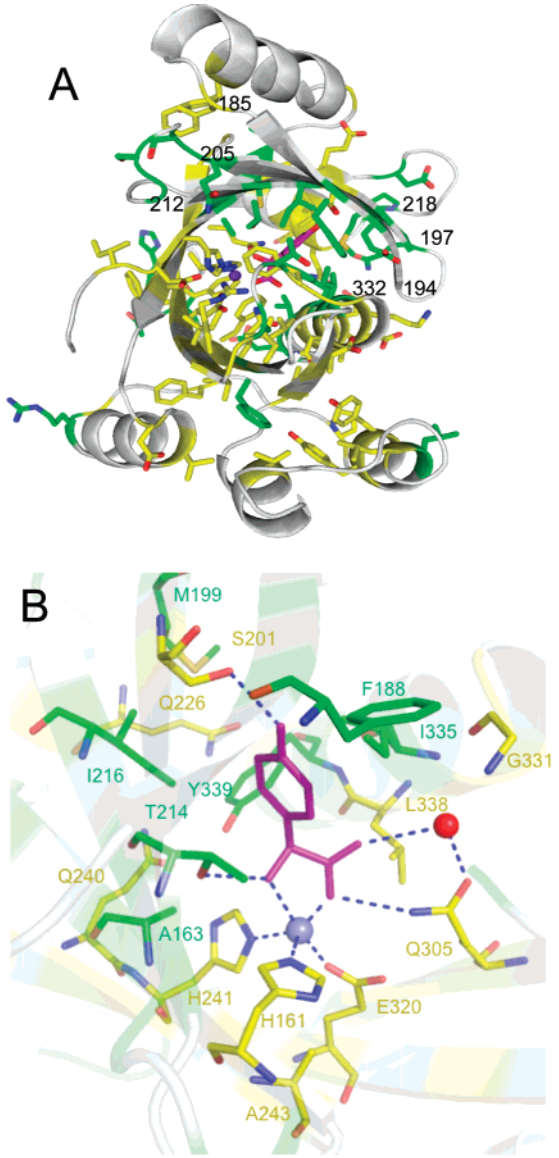

FIGURE 4: Hydroxymandelate binding site in HMS. (A) Clustering of HMS-specific residues about the phenol of the substrate in the context of the residues conserved in both HMS and HPPD. (B) Residues either in contact or proximal to the ligand. In both panels A and B, fully conserved residues have yellow carbon atoms and residues that are found in only HMS have their green carbon atoms. Hydroxymandelate is colored purple.

As a result of the additional carbon, the structure of HPP bows out away from Thr214 about 25° relative to the phenyl ring of HMA, placing the keto oxygen beyond hydrogen bonding distance (Figure 5A). While molecular dynamics and minimization had little effect on the manually modeled HMS·Fe^{2+}·HPP complex, in the minimized HPPD·Fe^{2+}·HPP complex, the position of the *p*-hydroxyl group of HPP is displaced by 4.5 Å relative to the position in the modeled HMS·Fe^{2+}·HPP complex (Figure 5B). This change in position puts the *p*-hydroxyl group in a completely different context, serving as a hydrogen bond acceptor for Ser201 and a hydrogen bond donor for the amide oxygen of Asn216. In addition, the molecular dynamics-minimized models also predict a change in the tilt angle of the planar α-keto carboxylate moiety of ∼27° and a change in the two torsion angles that lead to the phenol ring of about 15° and 30°, respectively.

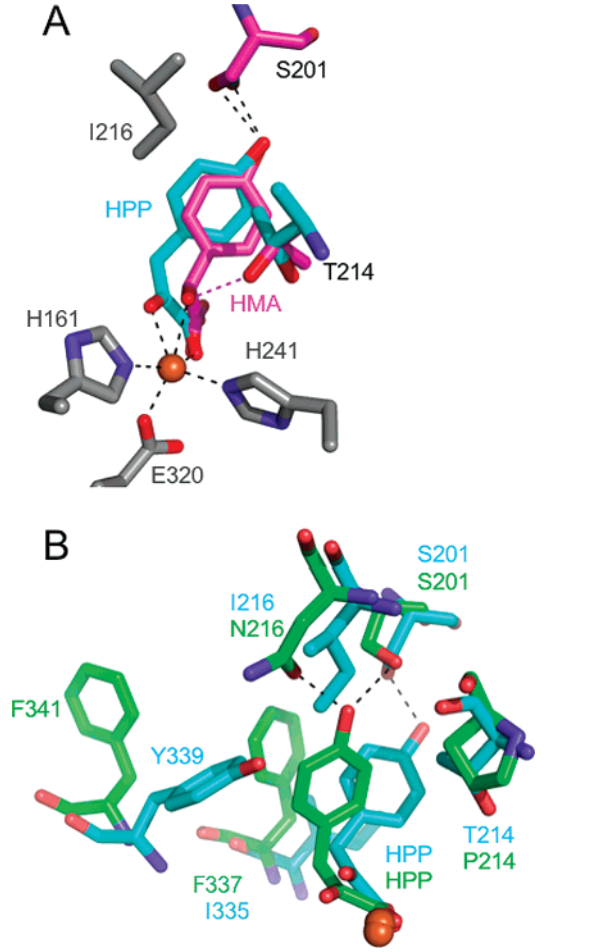

FIGURE 5: Ligand binding site predictions from molecular dynamics calculations. (A) Position of HPP (blue) and HMA (pink) in the structure of HMS. The rotational movement of the T214 side chain is depicted for each structure as is the position of the S201 residue. (B) Structure of HMS with HPP bound (blue structure) compared to the structure of *Pf*HPPD with HPP bound (green structure). The residue numbering is based on the primary structure of each sequence.

Models of HPP bound to variants of HPPD were also made to make correlations with the known activity of these mutated enzymes (Figure 6). The *p*-hydroxyl oxygens of the modeled HPP molecule in the F337I, P214T, and N216I variants show differences in position relative to that of the wild-type enzyme of 3.6, 1.9, and 2.4 Å, respectively. There is little change (0.4 Å) in the position of the *p*-hydroxyl oxygen of the HPP molecule of the F341Y variant relative to that of the wild-type enzyme. Interestingly, the position of the keto oxygen of the modeled HPP shows a 1.4 Å change in the two least active *Sa*HPPD variants (F337I and N216I) relative to the wild-type position, whereas the keto oxygens of the HPP from the other two variants are within 0.5 Å of the wild-type position.

DISCUSSION

Here we present the structure of HMS bound to its product HMA and modeling results that draw on these data. Modeling was done for the substrate complex of HMS, as well as substrate complexes of the related HPPD enzyme and several of its variants. These results shed light on the substrate binding mode of both HMS and HPPD and offer some rationalizations for the regiospecificities of the two enzymes.

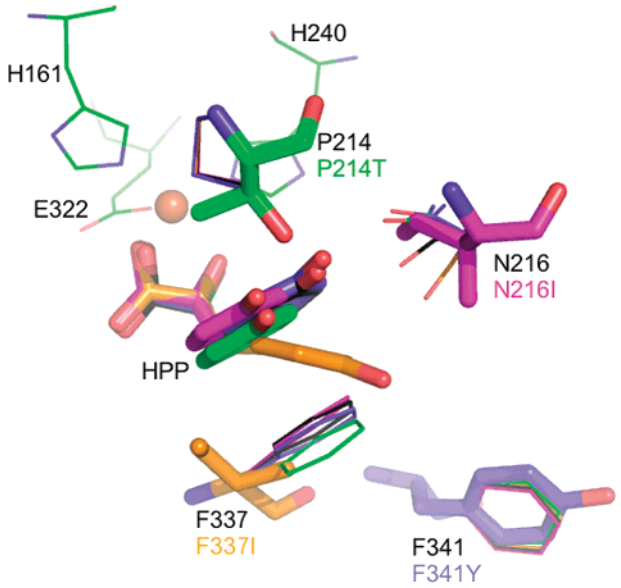

FIGURE 6: Models of HPP bound to the active site of variants of HPPD from *P. fluorescens* (PDB entry 1CJX). Colored black is the model of the wild-type enzyme bound to HPP, colored blue the F341Y mutated enzyme, colored green the P214T mutated enzyme, colored magenta the N216I mutated enzyme, and colored orange the F337I mutated enzyme. The residue numbering is based on the *P. fluorescens* sequence.

The level of sequence identity (as much as 35%) and similarity (as much as 50%) of the HMS and HPPD sequences is relatively high, as might be expected from two enzymes that share the same overall tertiary structure, perform a dioxygenation reaction, and require the same two substrates and whose reactions are believed to proceed through a common intermediate. On the basis of the structures and the sequence alignments of known HMSs and HPPDs, we conclude that proteins annotated as HPPD in sequence databases that contain 214-TLIExPD and 334-NI-(K/R)ALY motifs are more likely to have HMS activity. We assume that these sequence differences are in part responsible for their distinctly different products and their high degree of fidelity (*12*, *13*). The regiospecific hydroxylation found in the products suggests a significant degree of evolutionary divergence of the two enzymes, which has been previously proposed in phylogenetic analysis (*11*). This in turn raises the possibility that the binding orientation and/or conformation of the substrate HPP and/or intermediates is distinct in each enzyme, which had also been suggested previously (*18*). The assertion that hydroxylation regiospecificity is based in substrate and/or intermediate binding is reasonable if we accept that the primary hydroxylating intermediate is a ferryl−oxo species which has been observed in other αKAO enzymes (*27*−*32*) and that this intermediate is both potent and indiscriminate. Extensive evidence for the indiscriminate nature of the ferryl−oxo species can be found in αKAO enzymes that self-hydroxylate (*33*−*47*) and in those αKAO enzymes that catalyze multiple reactions using a single catalytic site (*48*−*50*). The requirement to deliver an oxygen atom to the benzylic carbon in the case of HMS or the aromatic ring in the case of HPPD would then be based largely on the orientation and proximity of the HPP-derived intermediate relative to the ferryl−oxo species.

HMS has a relatively large number of catalytic domain residues that are conserved yet distinct from HPPD such as those that start at positions 214 and 334. This suggests the existence of a distinct binding mode for the substrate phenol that is required to hold the aromatic ring away from a direct line of attack by the ferryl−oxo species. A proposed hypothesis illustrating the bifurcation of the reaction pathway toward the two activities is depicted in Scheme 2. This scheme is compiled from a number of earlier observations of HPPD, the structural data presented here, and observations of other mechanistically related enzymes. Catalysis is initiated by the bidentate association of HPP with the active site metal ion (*51*). This complex has elevated dioxygen reactivity (*13*, *52*) and delocalizes electron density from the planar α-keto acid of the pyruvate substituent to dioxygen via the metal ion (*53*). Dioxygen reduction occurs as individual one-electron steps to satisfy the requirement for spin inversion in the two-electron reduction of the dioxygen ground state triplet. This depletes the substrate of electrons and induces a nucleophilic attack at the HPP Cα atom to form an Fe(IV)-bridged peroxy species. Heterolytic (or homolytic) cleavage of the peroxy bond occurs concomitant with decarboxylation to yield the highly electrophilic Fe(IV)−oxo intermediate. It is proposed that it is at this point that the catalytic pathways of HMS and HPPD diverge. The ferryl−oxo species will either withdraw electrons from the aromatic ring or abstract a hydrogen atom from the benzylic carbon, depending how the enzyme positions the phenylacetate intermediate for attack. In the HPPD reaction pathway, localization of the arenium cation ortho to the aceto substituent would induce a substantial structural change corresponding to the shift of the side chain to form a dienone that then need only tautomerize to produce the product, HG. By contrast, in the HMS reaction pathway, the benzylic radical species can collapse with the ferric hydroxyl formed in the H-atom abstraction to form HMA directly.

The data presented here offer an explanation for how each reaction is accommodated and confined to occur exclusively in each catalytic cavity. The product HMA resembles the substrate HPP, and thus, the structure presented here is highly suggestive of the binding mode for HPP in HMS and an improved prediction for the HPPD−substrate complex (Figures 3A and 5A). These conclusions are supported by a number of additional observations. The presence of the conserved facial triad motif in the current Co^{2+}-substituted HMS structure and the fact that the product α-hydroxy acid makes a bidentate coordination with the active site metal ion in a manner analogous to the bidentate contact of the substrate α-keto acid (*5*−*10*, *18*, *49*, *51*, *53*−56) strengthen our confidence that the ligand-binding mode seen is catalytically relevant with respect to the substrate, HPP. Moreover, in such an orientation, the substrate carboxylate would lie in a *cis* position relative to Glu320's metal-coordinating carboxylate, consistent with what has been observed for the α-keto carboxylate of α-ketoglutarate in other αKAO enzymes (*7*−*10*, *49*, *54*, *56*).

Essentially all residues that contact the phenol of the product in the active site are uniquely conserved in HMS; this suggests that the enzyme is committed to capturing the phenol in this conformation with respect to the metal-coordinated pyruvate moiety. The hydrophobic pocket formed by these HMS-conserved residues follows closely the contour

Scheme 2

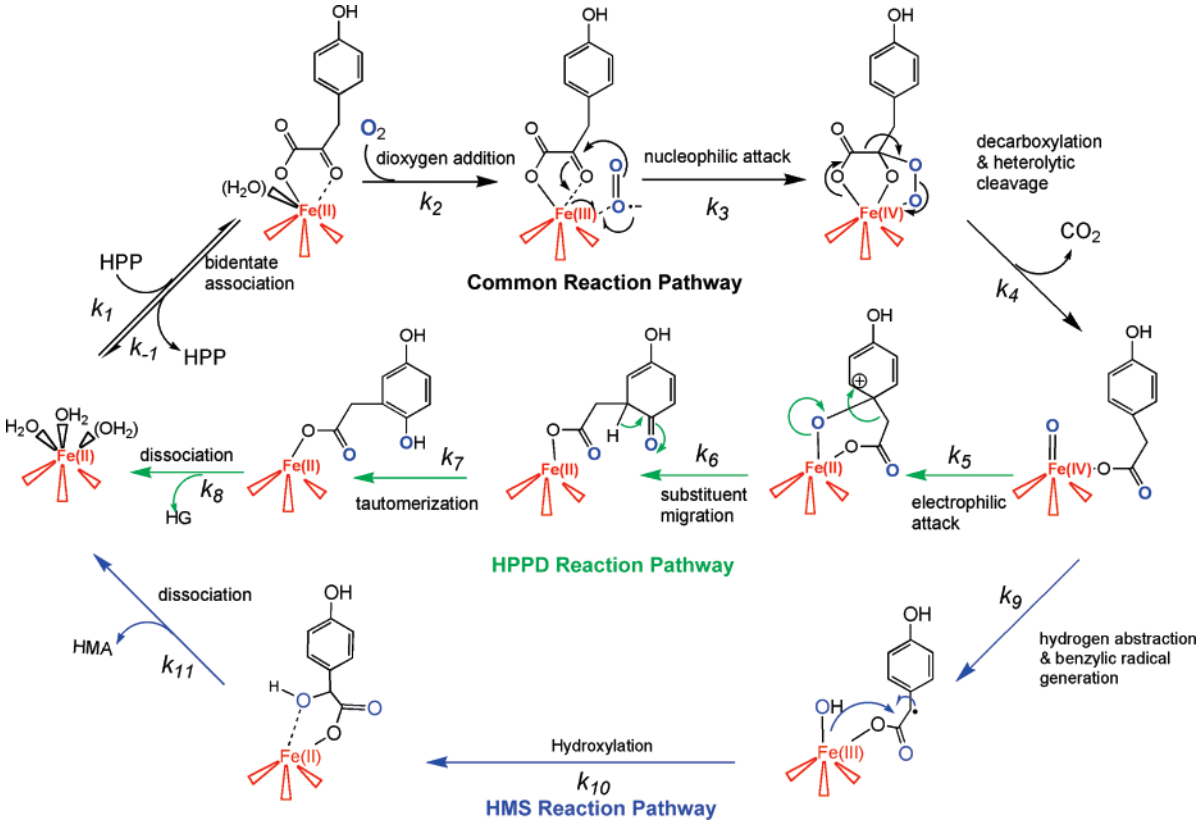

of the phenol's aromatic ring (Figure 4B, green residues). When the sample is held in this position, exposure of the benzylic carbon to the oxo group of the ferryl intermediate will require little deviation from the suggested substrate binding orientation and conformation. In the examination of 4-hydroxyphenylacetate binding to HMS and HPPD using density functional theory (DFT) calculations, Neidig et al. proposed that the π^* molecular orbital of the Fe^{4+}−oxo intermediate's oxygen atom overlaps well only with the benzylic carbon's C−H bond σ orbital from a sideways or orthogonal approach (*18*). If it is assumed that the product HMA's orientation and conformation in relation to the metal are not radically different from those of the proposed 4-hydroxyphenylacetate precursor intermediate, then one would reasonably guess that the position of the ferryl−oxo intermediate oxygen lies near the current position of the benzylic hydroxyl of HMA (Figures 3A and 5A). The benzylic hydroxyl is observed to hydrogen bond to the β-hydroxyl of Thr214, one of the residues conserved only in HMS sequences. Thr214 appears to serve multiple functions as the ethyl portion of its side chain constitutes part of the hydrophobic pocket enclosing the product phenol. At the same position in HPPD enzymes, a proline residue is universally observed. The molecular dynamics-minimized model of HPP bound to the active site of HMS suggests, however, that the keto oxygen does not form a hydrogen bond with Thr214 (Figure 5A). Instead, the primary role for this residue may be to correctly position the ferryl−oxo species for hydroxyl insertion onto the benzylic carbon. A reasonable hypothesis would predict that mutation of this residue would lower the positional hydroxylation specificity of HMS. However, for the inverse P214T mutation in HPPD, a novel product that arises from the resolution of an epoxide intermediate was detected rather than HMA (*11*).

Among the residues that are universally conserved in all known HMS and HPPD primary structures (Figures 1 and 4, yellow residues), Ser201 is remarkable. This is the only universally conserved residue in the β-sheet that contains residues 185−194, 197−205, 212−218 (Figure 4A), and its hydroxyl group is within hydrogen bonding distance of the *p*-hydroxyl of HMA (Figures 3A, 4B, and 5A). Given the shape similarity of HPP and HMA, this contact above all others suggests that the HMS structure presented offers an improved prediction for the substrate binding pocket in both HMS and HPPD, compared to that offered by earlier inhibitor complex structures (*1*, *23*). It may be ventured that, in HMS, Ser201 plays an anchoring role for the phenol to one extent or another throughout the entire reaction coordinate; indeed, Ser201 in modeled substrate complexes is observed to remain hydrogen bonded to the phenol hydroxyl throughout the 100 ps simulation (Figure 5A). In HPPD, Ser201 may serve a similar role in substrate−intermediate binding, though in select rather than all of the catalytic steps, since the transformation from substrate to product in this enzyme must involve greater structural change. Similar calculations based on the structure of HPPD from *P. fluorescens* with HPP bound suggest the additional participation of Asn216 in hydrogen bonding to the phenol hydroxyl in this enzyme (Figure 5B). Asn216 is fully conserved in HPPD sequences and is an isoleucine in HMS orthologs.

O'Hare et al. attempted to confer HPPD activity to the AoHMS protein by directed evolution aimed at five of the unique HPPD or HMS residues without success (*12*). One possible explanation for this is that, despite appearances, the

structures of HMS and HPPD are fundamentally different in that secondary structural elements containing residues that confer specificity are shifted by approximately 1 Å. The difference in the structural framework implies that single-point mutations designed to switch these specificity determinants are never likely to compensate for the overall shift in the structure. Gunsior et al. constructed four singly mutated HPPD enzymes that conferred attenuated but measurable native and/or altered activity (*11*). The behavior of these variants can be explained in part by the modeled substrate complexes. Specifically, the molecular dynamics-minimized modeled position of HPP in the F335I *Pf*HPPD variant is more similar to that in HMS than it is compared to any other HPPD variant (Figure 6). This is consistent with the observation of Gunsior et al. of measurable HMA activity for the corresponding F337I *Sa*HPPD variant. The nearly native activity of the F341Y variant is readily explained by the similarity in position of the modeled substrate relative to the wild type and ratifies the assumption made in the manual modeling that the tyrosine occupies the same position in the variant as it does in the wild-type enzyme. In HMS, the corresponding tyrosine makes van der Waals contact with the product. The observation of significant ring expoxidation activity in the P214T and F337I variant *Sa*HPPD enzymes cannot be directly addressed by the modeled substrate complexes other than noting that the substrate in both cases is modeled to be in a different position than in the wild-type enzyme. The lack of activity for the N216I variant may be explained by the fact that the modeled substrate in this case can form only one hydrogen bond to the *p*-hydroxy of the substrate, including that from Ser201, while all other variants have two hydrogen bonds. Additionally, the solvent accessible volume of the substrate binding site is smaller in this variant than that of any other variants and may result in a greater degree of unproductive binding.

By contrast, O'Hare et al. have seen that the HMS enzyme is quite tolerant to mutations since a large percentage of single and double mutants of the HMS gene at these four uniquely conserved locations retain an HMS phenotype (although, HMS activity itself was not measured). Importantly, none of these variants showed an HPPD phenotype. These observations can be rationalized by the small HMS substrate-binding site relative to that of HPPD (30 $Å^3$ for HMS vs 63 $Å^3$ for HPPD), where any mutation that does not exclude or retard HPP binding is likely to retain some amount of HMS catalysis, but still unlikely to accommodate the changes in positions required by the intermediates along the HPPD reaction pathway. Collectively, the mutation data support the theory that the active site of HMS is more restrictive for the phenol. This is further supported by a number of observations made with the wild-type forms of HPPD and HMS. First, HMS catalyzes mandelate production using phenylpyruvic acid (PPA) with a rate that is on the same order of magnitude as that with which it converts HPP to HMA, suggesting that the HPP *p*-hydroxyl is less important to the HMS reaction. Second, bacterial and plant HPPDs fail to make 2-hydroxyphenylacetate (2HPA), the analogue of HG, from PPA (*57*, *58*). The conclusion is, thus, absent the interaction with the conserved anchoring Ser201 the substrate is unanchored, eliminating the catalysis of decarboxylation and hence all subsequent chemistry.

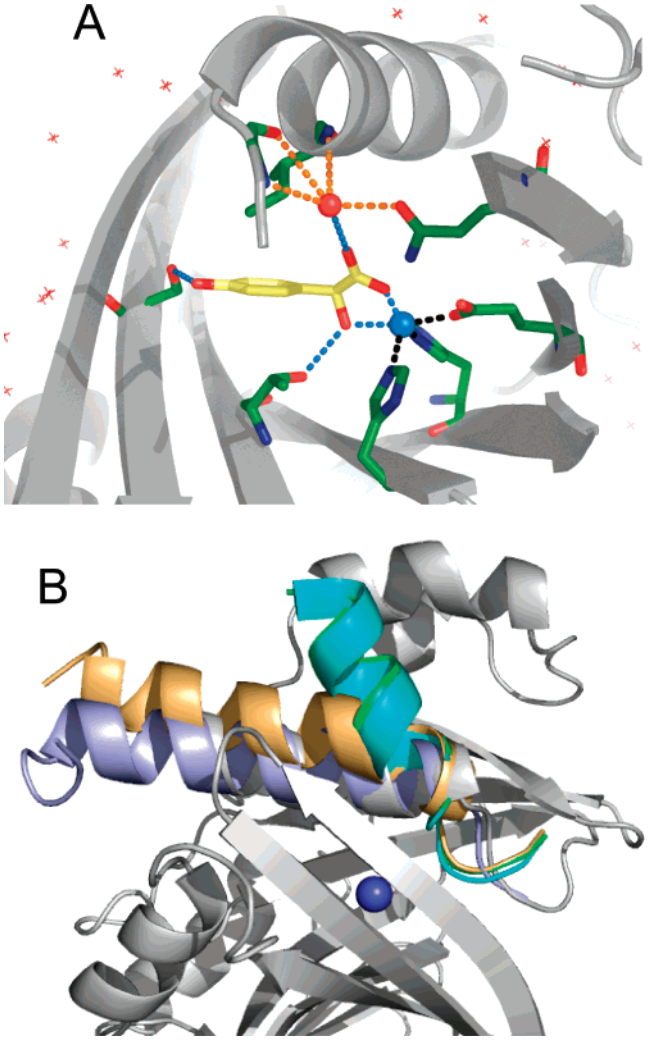

FIGURE 7: (A) Position of Water A with respect to the C-terminal helix (note that the C-terminus is oriented into the page). (B) Selection of C-terminal helix positions as observed in the structures of *A. orientalis* HMS (gray), *Arabidopsis thaliana* HPPD (green) with inhibitor 645 bound (*22*), *A. thaliana* HPPD (cyan) with no ligand bound (*22*), *Zea mays* HPPD (yellow beige) with no ligand bound (*24*), and *P. fluorescens* HPPD (pale lavender) with acetate bound (*21*). Note that an α-helix that in this view is just behind the C-terminal helix is omitted from all structures for clarity.

One other interesting set of interactions merits some mention. The product carboxylate comes in contact with two hydrogen-bonding entities, the universally conserved Gln305 and the highly ordered Water A (Figure 4). Interactions of this type were predicted from comparative DFT calculations correlated with MCD studies of the HMS− and HPPD− substrate complexes (*58*). Water A contacts the distal oxygen of the product carboxylate and resides at the N-terminal end of the C-terminal helix that covers and partly constitutes the active site of the enzyme (Figure 7A). In HPPD, this helix has been observed to adopt multiple conformations in the presence and absence of ligands (*21*−*24*) (Figure 7B). However, whether this α-helix is in a closed or open position does not correlate with either the presence of a ligand or the organismic origin of the enzyme. It has been suggested that this helix is a dynamic portion of the structure that gates access to the metal ion, and mobile structural elements that sequester the catalytic reaction from solvent have been proposed and/or demonstrated for many α-KAO enzymes

(*5*, *6*, *9*, *10*, *59*−*65*). It is interesting to note that Water A makes several contacts with residues that would lie at the hinge point for helix movement. In addition, in HPPD it has been shown that release of product HG is rate-limiting and sensitive in terms of rate to solvent-derived deuterons (*66*). If the final phase in HMS is the analogous product release step, Water A is a candidate to act as the general acid that donates a proton to the product and simultaneously influence the balance of energies that hold the C-terminal helix in position in the active site to promote displacement of the helix and release of the product, HMA.

In conclusion, the X-ray crystal structure of the HMA−HMS complex along with computational models of both the HPP−HMS and HPP−HPPD complexes has allowed us to assign a role for a conserved serine residue (Ser201), explain aspects of existing mutagenesis data in both HPPD and HMS, and propose a role for a newly identified buried water in the common product release step of both enzymes. We propose that, for either enzyme, proper positioning of the phenyl into the hydrophobic pocket is essential to catalysis, as this serves to orient the pyruvate α-keto acid moiety with respect to the metal ion and promote decarboxylation along with the generation of the ferryl−oxo intermediate. The divergent reactivity profiles are then due to HMS having a tighter hydrophobic pocket that does not permit the position of the phenyl ring to change greatly throughout the catalytic cycle. On the other hand, because the HPPD active site has need to accommodate a number of rather differently shaped structures due to the hydroxylation of the aromatic ring and the ensuing NIH shift, more space and conformational options for ligands must be built into its active site architecture.

ACKNOWLEDGMENT

The authors express their gratitude to Professor Christopher Walsh from Harvard Medical School for providing the gene for HMS from *A. orientalis*. We also thank Dr. Adam Stein and the Rosalind Franklin University X-ray facility for assistance in data collection and processing. Data were collected at Southeast Regional Collaborative Access Team (SER-CAT) 22 -ID beamline at the Advanced Photon Source, Argonne National Laboratory. Use of the Advanced Photon Source was supported by the U.S. Department of Energy, Office of Science, Office of Basic Energy Sciences, under Contract W-31-109-Eng-38.

REFERENCES

1. Moran, G. R. (2005) 4-Hydroxyphenylpyruvate dioxygenase, *Arch. Biochem. Biophys. 433*, 117−128.
2. Choroba, O. W., Williams, D. H., and Spencer, J. B. (2000) Biosynthesis of the vancomycin group of antibiotics: Involvement of an unusual dioxygenase in the pathway to (S)-4-hydroxyphenylglycine, *J. Am. Chem. Soc. 122*, 5389−5390.
3. Hubbard, B. K., Thomas, M. G., and Walsh, C. T. (2000) Biosynthesis of L-p-hydroxyphenylglycine, a non-proteinogenic amino acid constituent of peptide antibiotics, *Chem. Biol. 7*, 931−942.
4. Purpero, V., and Moran, G. R. (2007) The diverse and pervasive chemistries of the α-keto acid dependent enzymes, *J. Biol. Inorg. Chem. 12*, 587−601.
5. Muller, I., Kahnert, A., Pape, T., Sheldrick, G. M., Meyer-Klaucke, W., Dierks, T., Kertesz, M., and Uson, I. (2004) Crystal structure of the alkylsulfatase AtsK: Insights into the catalytic mechanism of the Fe(II) α-ketoglutarate-dependent dioxygenase superfamily, *Biochemistry 43*, 3075−3088.
6. Zhang, Z., Ren, J., Stammers, D. K., Baldwin, J. E., Harlos, K., and Schofield, C. J. (2000) Structural origins of the selectivity of the trifunctional oxygenase clavaminic acid synthase, *Nat. Struct. Biol. 7*, 127−133.
7. Dann, C. E., III, Bruick, R. K., and Deisenhofer, J. (2002) Structure of factor-inhibiting hypoxia-inducible factor 1: An asparaginyl hydroxylase involved in the hypoxic response pathway, *Proc. Natl. Acad. Sci. U.S.A. 99*, 15351−15356.
8. Elkins, J. M., Hewitson, K. S., McNeill, L. A., Seibel, J. F., Schlemminger, I., Pugh, C. W., Ratcliffe, P. J., and Schofield, C. J. (2003) Structure of factor-inhibiting hypoxia-inducible factor (HIF) reveals mechanism of oxidative modification of HIF-1α, *J. Biol. Chem. 278*, 1802−1806.
9. Clifton, I. J., Doan, L. X., Sleeman, M. C., Topf, M., Suzuki, H., Wilmouth, R. C., and Schofield, C. J. (2003) Crystal structure of carbapenem synthase (CarC), *J. Biol. Chem. 278*, 20843−20850.
10. McDonough, M. A., Kavanagh, K. L., Butler, D., Searls, T., Oppermann, U., and Schofield, C. J. (2005) Structure of human phytanoyl-CoA 2-hydroxylase identifies molecular mechanisms of Refsum disease, *J. Biol. Chem. 280*, 41101−41110.
11. Gunsior, M., Ravel, J., Challis, G. L., and Townsend, C. A. (2004) Engineering p-hydroxyphenylpyruvate dioxygenase to a p-hydroxymandelate synthase and evidence for the proposed benzene oxide intermediate in homogentisate formation, *Biochemistry 43*, 663−674.
12. O'Hare, H. M., Huang, F., Holding, A., Choroba, O. W., and Spencer, J. B. (2006) Conversion of hydroxyphenylpyruvate dioxygenases into hydroxymandelate synthases by directed evolution, *FEBS Lett. 580*, 3445−3450.
13. Johnson-Winters, K., Purpero, V. M., Kavana, M., Nelson, T., and Moran, G. R. (2003) (4-Hydroxyphenyl)pyruvate Dioxygenase from *Streptomyces avermitilis*: The Basis for Ordered Substrate Addition, *Biochemistry 42*, 2072−2080.
14. Terwilliger, T. C. (1997) Multiwavelength anomalous diffraction phasing of macromolecular structures: Analysis of MAD data as single isomorphous replacement with anomalous scattering data using the MADMRG Program, *Methods Enzymol. 276*, 530−537.
15. Terwilliger, T. (2004) SOLVE and RESOLVE: Automated structure solution, density modification and model building, *J. Synchrotron Radiat. 11*, 49−52.
16. Jones, T. A., Zou, J. Y., Cowan, S. W., and Kjeldgaard, M. (1991) Improved methods for building protein models in electron density maps and the location of errors in these models, *Acta Crystallogr. A47* (Part 2), 110−119.
17. Brunger, A. T., Adams, P. D., Clore, G. M., DeLano, W. L., Gros, P., Grosse-Kunstleve, R. W., Jiang, J. S., Kuszewski, J., Nilges, M., Pannu, N. S., Read, R. J., Rice, L. M., Simonson, T., and Warren, G. L. (1998) Crystallography & NMR system: A new software suite for macromolecular structure determination, *Acta Crystallogr. D54*, 905−921.
18. Neidig, M. L., Decker, A., Choroba, O. W., Huang, F., Kavana, M., Moran, G. R., Spencer, J. B., and Solomon, E. I. (2006) Spectroscopic and electronic structure studies of aromatic electrophilic attack and hydrogen-atom abstraction by non-heme iron enzymes, *Proc. Natl. Acad. Sci. U.S.A. 103*, 12966−12973.
19. Studier, F. W., Rosenberg, A. H., Dunn, J. J., and Dubendorff, J. W. (1990) Use of T7 RNA polymerase to direct expression of cloned genes, *Methods Enzymol. 185*, 60−89.
20. Luzatti, V. (1952) Traitement statistique des erreurs dans la determination des structures cristallines, *Acta Crystallogr. 5*, 802−810.
21. Serre, L., Sailland, A., Sy, D., Boudec, P., Rolland, A., Pebay-Peyroula, E., and Cohen-Addad, C. (1999) Crystal structure of *Pseudomonas fluorescens* 4-hydroxyphenylpyruvate dioxygenase: An enzyme involved in the tyrosine degradation pathway, *Struct. Folding Des. 7*, 977−988.
22. Yang, C., Pflugrath, J. W., Camper, D. L., Foster, M. L., Pernich, D. J., and Walsh, T. A. (2004) Structural Basis for Herbicidal Inhibitor Selectivity Revealed by Comparison of Crystal Structures of Plant and Mammalian 4-Hydroxyphenylpyruvate Dioxygenases, *Biochemistry 43*, 10414−10423.
23. Brownlee, J., Johnson-Winters, K., Harrison, D. H. T., and Moran, G. R. (2004) The Structure of the Ferrous Form of (4−Hydroxyphenyl)pyruvate Dioxygenase from *Streptomyces avermitilis* in Complex with the Therapeutic Herbicide, NTBC, *Biochemistry 43*, 6370−6377.
24. Fritze, I. M., Linden, L., Freigang, J., Auerbach, G., Huber, R., and Steinbacher, S. (2004) The crystal structures of *Zea mays*

and *Arabidopsis* 4-hydroxyphenylpyruvate dioxygenase, *Plant Physiol. 134*, 1388−1400.
25. Han, S., Eltis, L. D., Timmis, K. N., Muchmore, S. W., and Bolin, J. T. (1995) Crystal structure of the biphenyl-cleaving extradiol dioxygenase from a PCB-degrading pseudomonad, *Science 270*, 976−980.
26. Eltis, L. D., and Bolin, J. T. (1996) Evolutionary relationships among extradiol dioxygenases, *J. Bacteriol. 178*, 5930−5937.
27. Riggs-Gelasco, P. J., Price, J. C., Guyer, R. B., Brehm, J. H., Barr, E. W., Bollinger, J. M., Jr., and Krebs, C. (2004) EXAFS spectroscopic evidence for an Fe=O unit in the Fe(IV) intermediate observed during oxygen activation by taurine:α-ketoglutarate dioxygenase, *J. Am. Chem. Soc. 126*, 8108−8109.
28. Price, J. C., Barr, E. W., Tirupati, B., Bollinger, J. M., Jr., and Krebs, C. (2003) The first direct characterization of a high-valent iron intermediate in the reaction of an α-ketoglutarate-dependent dioxygenase: A high-spin FeIV complex in taurine/α-ketoglutarate dioxygenase (TauD) from *Escherichia coli*, *Biochemistry 42*, 7497−7508.
29. Price, J. C., Barr, E. W., Glass, T. E., Krebs, C., and Bollinger, J. M., Jr. (2003) Evidence for hydrogen abstraction from C1 of taurine by the high-spin Fe(IV) intermediate detected during oxygen activation by taurine:α-ketoglutarate dioxygenase (TauD), *J. Am. Chem. Soc. 125*, 13008−13009.
30. Galonic, D. P., Barr, E. W., Walsh, C. T., Bollinger, J. M., Jr., and Krebs, C. (2007) Two interconverting Fe(IV) intermediates in aliphatic chlorination by the halogenase CytC3, *Nat. Chem. Biol. 3*, 113−116.
31. Hoffart, L. M., Barr, E. W., Guyer, R. B., Bollinger, J. M., Jr., and Krebs, C. (2006) Direct spectroscopic detection of a C-H-cleaving high-spin Fe(IV) complex in a prolyl-4-hydroxylase, *Proc. Natl. Acad. Sci. U.S.A. 103*, 14738−14743.
32. Proshlyakov, D. A., Henshaw, T. F., Monterosso, G. R., Ryle, M. J., and Hausinger, R. P. (2004) Direct detection of oxygen intermediates in the non-heme Fe enzyme taurine/α-ketoglutarate dioxygenase, *J. Am. Chem. Soc. 126*, 1022−1023.
33. Tuderman, L., Myllyla, R., and Kivirikko, K. I. (1977) Mechanism of the prolyl hydroxylase reaction. 1. Role of co-substrates, *Eur. J. Biochem. 80*, 341−348.
34. Myllyla, R., Kuutti-Savolainen, E. R., and Kivirikko, K. I. (1978) The role of ascorbate in the prolyl hydroxylase reaction, *Biochem. Biophys. Res. Commun. 83*, 441−448.
35. Ge, Y., Lawhorn, B. G., ElNaggar, M., Sze, S. K., Begley, T. P., and McLafferty, F. W. (2003) Detection of four oxidation sites in viral prolyl-4-hydroxylase by top-down mass spectrometry, *Protein Sci. 12*, 2320−2326.
36. Rao, N. V., and Adams, E. (1978) Partial reaction of prolyl hydroxylase. $(Gly\text{-}PRO\text{-}Ala)_n$ stimulates α-ketoglutarate decarboxylation without prolyl hydroxylation, *J. Biol. Chem. 253*, 6327−6330.
37. De Jong, L., and Kemp, A. (1984) Stoicheiometry and kinetics of the prolyl 4-hydroxylase partial reaction, *Biochim. Biophys. Acta 787*, 105−111.
38. Counts, D. F., Cardinale, G. J., and Udenfriend, S. (1978) Prolyl hydroxylase half reaction: Peptidyl prolyl-independent decarboxylation of α-ketoglutarate, *Proc. Natl. Acad. Sci. U.S.A. 75*, 2145−2149.
39. Holme, E., and Lindstedt, S. (1982) Studies on the partial reaction of thymine 7-hydroxylase in the presence of 5-fluorouracil, *Biochim. Biophys. Acta 704*, 278−283.
40. Myllyharju, J., and Kivirikko, K. I. (1997) Characterization of the iron- and 2-oxoglutarate-binding sites of human prolyl 4-hydroxylase, *EMBO J. 16*, 1173−1180.
41. Lindstedt, S., and Rundgren, M. (1982) Blue color, metal content, and substrate binding in 4-hydroxyphenylpyruvate dioxygenase from *Pseudomonas* sp. strain P. J. 874, *J. Biol. Chem. 257*, 11922−11931.
42. Bradley, F. C., Lindstedt, S., Lipscomb, J. D., Que, L., Jr., Roe, A. L., and Rundgren, M. (1986) 4-Hydroxyphenylpyruvate dioxygenase is an iron-tyrosinate protein, *J. Biol. Chem. 261*, 11693−11696.
43. Liu, A., Ho, R. Y., Que, L., Ryle, M. J., Phinney, B. S., and Hausinger, R. P. (2001) Alternative Reactivity of an α-Ketoglutarate-Dependent Iron(II) Oxygenase: Enzyme Self-Hydroxylation, *J. Am. Chem. Soc. 123*, 5126−5127.
44. Ryle, M. J., Liu, A., Muthukumaran, R. B., Ho, R. Y., Koehntop, K. D., McCracken, J., Que, L., Jr., and Hausinger, R. P. (2003) O2- and α-ketoglutarate-dependent tyrosyl radical formation in TauD, an α-keto acid-dependent non-heme iron dioxygenase, *Biochemistry 42*, 1854−1862.
45. Ryle, M. J., Koehntop, K. D., Liu, A. M., Que, L., and Hausinger, R. P. (2003) Interconversion of two oxidized forms of taurine/α-ketoglutarate dioxygenase, a non-heme iron hydroxylase: Evidence for bicarbonate binding, *Proc. Natl. Acad. Sci. U.S.A. 100*, 3790−3795.
46. Henshaw, T. F., Feig, M., and Hausinger, R. P. (2004) Aberrant activity of the DNA repair enzyme AlkB, *J. Inorg. Biochem. 98*, 856−861.
47. Sundheim, O., Vagbo, C. B., Bjoras, M., Sousa, M. M., Talstad, V., Aas, P. A., Drablos, F., Krokan, H. E., Tainer, J. A., and Slupphaug, G. (2006) Human ABH3 structure and key residues for oxidative demethylation to reverse DNA/RNA damage, *EMBO J. 25*, 3389−3397.
48. Zhang, Z., Ren, J., Harlos, K., McKinnon, C. H., Clifton, I. J., and Schofield, C. J. (2002) Crystal structure of a clavaminate synthase-Fe(II)-2-oxoglutarate-substrate-NO complex: Evidence for metal centred rearrangements, *FEBS Lett. 517*, 7−12.
49. Zhou, J., Kelly, W. L., Bachmann, B. O., Gunsior, M., Townsend, C. A., and Solomon, E. I. (2001) Spectroscopic studies of substrate interactions with clavaminate synthase 2, a multifunctional α-KG-dependent non-heme iron enzyme: Correlation with mechanisms and reactivities, *J. Am. Chem. Soc. 123*, 7388−7398.
50. Lloyd, M. D., Merritt, K. D., Lee, V., Sewell, T. J., Wha-Son, B., Baldwin, J. E., and Schofield, C. J. (1999) Product-Substrate Engineering by Bacteria: Studies on Clavaminate Synthase, a Trifunctional Dioxygenase, *Tetrahedron 55*, 10201−10220.
51. Neidig, M. L., Kavana, M., Moran, G. R., and Solomon, E. I. (2004) CD and MCD Studies of the Non-Heme Ferrous Active Site in (4-Hydroxyphenyl)pyruvate Dioxygenase: Correlation Between Oxygen Activation in the Extradiol and α-KG Dependent Dioxygenases, *J. Am. Chem. Soc. 126*, 4486−4487.
52. Rundgren, M. (1977) Steady state kinetics of 4-hydroxyphenylpyruvate dioxygenase from human liver (III), *J. Biol. Chem. 252*, 5094−5099.
53. Pavel, E. G., Zhou, J., Busby, R. W., Gunsior, M., Townsend, C. A., and Solomon, E. I. (1998) Circular Dichroism and Magnetic Circular Dichroism Spectroscopic Studies of the Non-Heme Ferrous Active Site in Clavaminate Synthase and Its Interaction with α-Ketoglutarate Cosubstrate, *J. Am. Chem. Soc. 120*, 743−753.
54. Valegard, K., van Scheltinga, A. C., Lloyd, M. D., Hara, T., Ramaswamy, S., Perrakis, A., Thompson, A., Lee, H. J., Baldwin, J. E., Schofield, C. J., Hajdu, J., and Andersson, I. (1998) Structure of a cephalosporin synthase, *Nature 394*, 805−809.
55. Solomon, E. I., Decker, A., and Lehnert, N. (2003) Bioinorganic Chemistry Special Feature: Non-heme iron enzymes: Contrasts to heme catalysis, *Proc. Natl. Acad. Sci. U.S.A. 100*, 3589−3594.
56. Ho, R. Y., Mehn, M. P., Hegg, E. L., Liu, A., Ryle, M. J., Hausinger, R. P., and Que, L., Jr. (2001) Resonance Raman studies of the iron(II)−α-keto acid chromophore in model and enzyme complexes, *J. Am. Chem. Soc. 123*, 5022−5029.
57. Purpero, V. M., and Moran, G. R. (2006) Catalytic, noncatalytic, and inhibitory phenomena: Kinetic analysis of (4-hydroxyphenyl)-pyruvate dioxygenase from *Arabidopsis thaliana*, *Biochemistry 45*, 6044−6055.
58. Neidig, M. L., Brown, C. D., Kavana, M., Choroba, O. W., Spencer, J. B., Moran, G. R., and Solomon, E. I. (2006) Spectroscopic and electronic structure studies of the role of active site interactions in the decarboxylation reaction of α-keto acid-dependent dioxygenases, *J. Inorg. Biochem. 100*, 2108−2116.
59. Lange, T., Kegler, C., Hedden, P., Phillips, A. L., and Graebe, J. E. (1997) Molecular characterisation of gibberellin 20-oxidases. Structure-function studies on recombinant enzymes and chimaeric proteins, *Physiol. Plant. 100*, 543−549.
60. Wilmouth, R. C., Turnbull, J. J., Welford, R. W., Clifton, I. J., Prescott, A. G., and Schofield, C. J. (2002) Structure and mechanism of anthocyanidin synthase from *Arabidopsis thaliana*, *Structure 10*, 93−103.
61. Oster, L. M., van Scheltinga, A. C., Valegard, K., Hose, A. M., Dubus, A., Hajdu, J., and Andersson, I. (2004) Conformational flexibility of the C terminus with implications for substrate binding and catalysis revealed in a new crystal form of deacetoxycephalosporin C synthase, *J. Mol. Biol. 343*, 157−171.
62. Lee, H. J., Lloyd, M. D., Harlos, K., Clifton, I. J., Baldwin, J. E., and Schofield, C. J. (2001) Kinetic and crystallographic studies

on deacetoxycephalosporin C synthase (DAOCS), *J. Mol. Biol. 308*, 937−948.
63. Lloyd, M. D., Lee, H. J., Harlos, K., Zhang, Z. H., Baldwin, J. E., Schofield, C. J., Charnock, J. M., Garner, C. D., Hara, T., Terwisscha van Scheltinga, A. C., Valegard, K., Viklund, J. A., Hajdu, J., Andersson, I., Danielsson, A., and Bhikhabhai, R. (1999) Studies on the active site of deacetoxycephalosporin C synthase, *J. Mol. Biol. 287*, 943−960.
64. Valegard, K., Terwisscha van Scheltinga, A. C., Dubus, A., Ranghino, G., Oster, L. M., Hajdu, J., and Andersson, I. (2004) The structural basis of cephalosporin formation in a mononuclear ferrous enzyme, *Nat. Struct. Mol. Biol. 11*, 95−101.
65. Yu, B., Edstrom, W. C., Benach, J., Hamuro, Y., Weber, P. C., Gibney, B. R., and Hunt, J. F. (2006) Crystal structures of catalytic complexes of the oxidative DNA/RNA repair enzyme AlkB, *Nature 439*, 879−884.
66. Johnson-Winters, K., Purpero, V. M., Kavana, M., and Moran, G. R. (2005) Accumulation of Multiple Intermediates in the Catalytic Cycle of (4-Hydroxyphenyl)pyruvate Dioxygenase from *Streptomyces avermitilis*, *Biochemistry 44*, 7189−7199.
67. Laskowski, R. A., Macarthur, M. W., Moss, D. S., and Thornton, J. M. (1993) Procheck: A Program to Check the Stereochemical Quality of Protein Structures, *J. Appl. Crystallogr. 26*, 283−291.
68. Engh, R. A., and Huber, R. (1991) Accurate Bond and Angle Parameters for X-Ray Protein-Structure Refinement, *Acta Crystallogr. A47*, 392−400.

BI701438R